Eur. Phys. J. A (2016) **52**: 126
DOI 10.1140/epja/i2016-16126-x

THE EUROPEAN PHYSICAL JOURNAL A

Regular Article – Experimental Physics

Measurements of conversion electrons in the s-process branching point nucleus ^{176}Lu

A. Battaglia[a], W. Tan, R. Avetisyan, C. Casarella, A. Gyurijinyan, K.V. Manukyan, S.T. Marley, A. Nystrom, N. Paul, K. Siegl, K. Smith, M.K. Smith, S.Y. Strauss, and A. Aprahamian

Department of Physics, University of Notre Dame, Notre Dame, IN, 46556, USA

Received: 22 December 2015 / Revised: 6 March 2016
Published online: 12 May 2016 –
Communicated by Alexandra Gade

Abstract. Conversion coefficients, gamma-gamma and gamma-electron coincidences were measured in the s-process branching point nucleus ^{176}Lu. Our goal was to determine the multipolarities of the γ-ray transitions that connect the high and low K states of ^{176}Lu. This ^{176}Lu nucleus has a long-lived ground state ($K = 7^-$) of 37.6 Gy, a short-lived isomeric state ($K = 0^-$) at 122.8 keV with half-life of 3.6 h, as well as a 58 μs isomer at 1588 keV ($K = 14^+$). The excitation structure of this nucleus contains bands of intermediate spins of both positive and negative parities. The intermediate states can under certain stellar temperatures completely change the equilibrium between the isomer and ground state of ^{176}Lu and change the abundance of this nucleus. We populated 37 previously known levels in this nucleus via the ^{176}Yb(p, n) reaction and measured 42 conversion coefficients for γ-ray transitions including 17 of them for the first time.

1 Introduction

The formation of heavy elements beyond iron is predominately via neutron capture processes, the slow (s-process) [1–3] and the rapid (r-process) [4] capture processes. The site of the r-process remains one of the open challenges in all of physics [5] where the r-process elemental abundances are one of the most crucial ingredients in determining the embedded nuclear physics and clues towards a potential site(s) for the r-process. The r-process abundance distributions are typically determined through the subtraction of the observed solar abundances from the s-process nuclei abundances [4] and sometimes directly from observations of metal poor stars [6]. Critical to a reliable r-process abundance distribution is the precise knowledge of the s-process nuclei and their contributions [7]. The s-process runs along the valley of stability whereas the r-process takes place far from stability with β-decays towards the line of stability frequently adding to the elemental abundances of both s- and r-process subsets of nuclei. Nuclei can in principle be of both r- and s-process origin (*e.g.* ^{175}Yb and ^{177}Hf). Therefore, nuclei of pure r- or s-process origin are of great interest for determining the final abundances. There are some 15 or so nuclei that show some separation and branching between the s- and r-process, and the ^{176}Lu nucleus is one of them [1]. The ^{176}Lu nucleus was considered an s-only nucleus due to the shielding from β-decay of the r-process by its stable isobar ^{176}Yb as shown in fig. 1 [2]. The ^{176}Lu nucleus has a ground state of ($J^\pi = 7^-$, $K = 7$) with a half-life of 37.6 Gy [8], and an isomeric state at 122.8 keV ($J^\pi = 1^-$, $K = 0$) with a half-life of 3.635 hrs [8]. The configuration of the $K^\pi = 7^-$ state is thought to be $\pi 7/2^+[404] \otimes \nu 7/2^-[512]$ and the origin of the $K^\pi = 0^-$ state is the antiparallel coupling of the same configuration [9,10]. There is likely no direct link between the two states due to the high level of K-forbiddeness. Audouze and Fowler [11] had postulated that ^{176}Lu could be a candidate for a long-lived galactic chronometer given its shielding from the r-process by ^{176}Yb. The ground state was thought to provide a measure of the age of s-process generated nuclei in the solar system [12]. However, the low-lying isomeric state complicates the role of ^{176}Lu in stellar environments. In these stellar environments, nuclei are exposed to high temperatures on the order of 10^8 K which can populate levels up to ~ 1 MeV [3,13,14]. This thermal excitation would impact the abundance of ^{176}Lu in the s-process. If the low-spin isomer at 122.8 keV is populated, the decay on a relatively short time scale would decrease the abundance, whereas if higher excitation and spin states are populated then the decay would go to the long-lived ground state increasing the abundance [9].

There were also a number of studies that showed the existence of high K isomers of 14^+ and 12^+ as well as a number of other bands of intermediate spin of both positive and negative parity in this nucleus [9,13,15,16].

[a] e-mail: abattagl@nd.edu

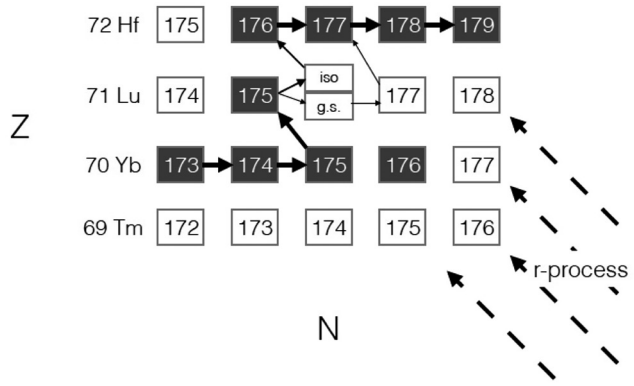

Fig. 1. A representation of the r- and s-process path near $A \sim 176$ is shown. The solid black line is the s-process path and shows the shielding of ^{176}Lu from the stable ^{176}Yb.

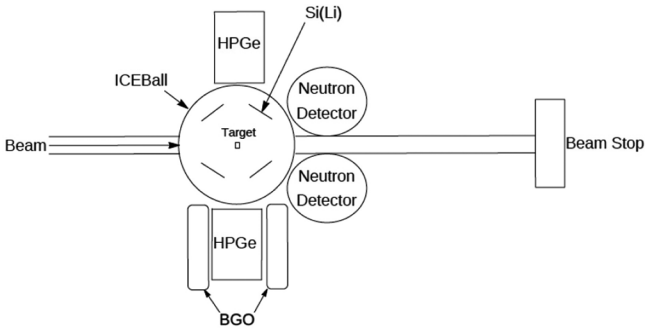

Fig. 2. The experimental setup of this experiment using the ICEBALL array of Si(Li) detectors, 2 HPGe detectors, and 2 neutron scintillators. ICEBall is shown from a top down perspective showing 4 of the 6 Si(Li) detectors, the other two detectors are at the top and bottom centered over the target.

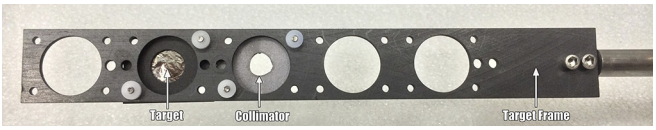

Fig. 3. The carbon target ladder shown with a target frame, and collimator. The collimator is made out of tantalum and was used for beam tuning. All calibration sources were mounted on the same ladder to insure centering in the ICEBAll array.

Transitions from intermediate spin states would effectively reduce the K-forbiddenness by connecting states of very low and very high K. The strength of the transitions connecting the intermediate states with the isomeric states or the ground state would impact the resulting abundance [13]. This is the goal of the present work. Earlier studies had suggested already that an additional mechanism such as, intermediate states that communicate to both the ground state and the isomer, are necessary to reproduce the observed ^{176}Lu abundance [8,12,17–19]. An intermediate state in the $K^\pi = 4^-$ band was first identified by Klay *et al.* at 839 keV [15] and was later verified by Lesko *et al.* [13], with a lifetime of $\tau \geq 10$ ps [20,21]. The lifetime of this intermediate state is thought to constrain the thermal equilibration between the ground and isomeric state even at lower temperatures in stellar environments [22]. As an aside, the identification of an intermediate state nullified the use of ^{176}Lu as a chronometer but still held some applicability of this nucleus as a stellar thermometer [13–15,20,23]. Recent studies by McGoram *et al.* [16] using the ^{176}Yb(^{7}Li,$\alpha 3n$) reaction established a high-lying level structure that populated levels up to 1588 keV and spins up to $K = 14^+$. The high-lying level scheme that was established was then used in a subsequent study by Dracoulis *et al.* [9] using the ^{176}Lu + ^{136}Xe inelastic reaction. Dracoulis *et al.* identified five additional members in the $K^\pi = 4^+$ band, that communicate to both the ground state and isomeric state. The lowest-lying intermediate state identified by Dracoulis *et al.* is at 709 keV [9].

Our goal in this experiment was to populate as many of the intermediate states as possible in both the $K^\pi = 4^-$ and $K^\pi = 4^+$ bands to determine the multipolarities of the γ-ray transitions connecting the intermediate states to the states of high and low K levels by measuring their conversion coefficients.

2 Experiment

We measured conversion coefficients of γ-rays depopulating excited levels in ^{176}Lu following the ^{176}Yb$(p,n)^{176}$Lu reaction. The experiment was carried out at the Nuclear Science Laboratory of the University of Notre Dame using the FN-Tandem accelerator. The proton beam energy was 7.75 MeV with an intensity of 1 electron nA on average, and bunched with a period of $\sim 1\,\mu$s. The beam energy was chosen to maximize the yield of ^{176}Lu while minimizing other reaction channels. The target consisted of a 1.37 mg/cm^2 metallic ^{176}Yb foil enriched to 97% [1]. We measured γ-rays, neutrons, and electrons. Figure 2 illustrates the arrangement of the detectors for this experiment. Conversion electrons were measured with the Internal Conversion Electron Ball Array (ICEBall). ICEBall was initially developed by J.X. Saladin and M.P. Metlay at the University of Pittsburgh [24] and recently recommissioned at the University of Notre Dame (ND). ICEBall at ND has undergone multiple upgrades to improve its overall efficiency from 6% to 15% over 4π at 356 keV, a more efficient cooling system has been developed, and all Si(Li) detectors have been repaired. The experimental setup included two high-purity germanium (HPGe) detectors (109% relative efficiency, 0.42% absolute efficiency at 356 keV) from the GErmanium detector Online aRray for Gamma ray spectroscopy in Nuclear Astrophysics (GEORGINA) array, and two NE213 liquid organic scintillators (hexagonal 12.5 cm thick) for measuring and monitoring the neutron flux. The target as well as the calibration sources were placed on a ladder system centered in the ICEBall array. The target frame and ladder were made of carbon to reduce the beam induced background with thicknesses of 0.7 mm and 1.5 mm, respectively. Figure 3 shows the target ladder used in this ex-

[1] Oak Ridge National Laboratory, ^{176}Yb oxide, batch number: 218801, isotope order number: 47-0023.

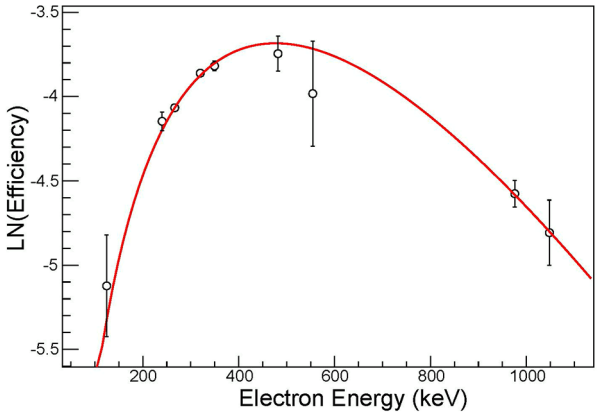

Fig. 4. A single Si(Li) efficiency curve using two calibration sources ^{133}Ba and ^{207}Bi placed at the center of ICEBall.

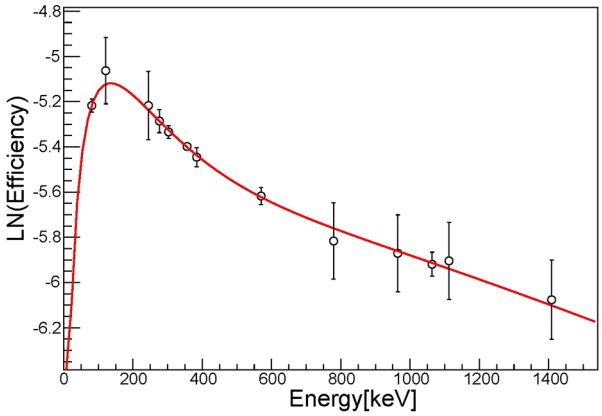

Fig. 5. A single HPGe detector efficiency curve determined by using three calibration sources ^{133}Ba, ^{152}Eu, and ^{207}Bi. The ^{133}Ba and the ^{207}Bi sources were placed at the center of ICEBall target position, while the ^{152}Eu was placed outside ICEBall and normalized to the other sources.

periment. One of the HPGe detectors was actively shielded with an early Gammasphere prototype BGO detector [25] borrowed from the Argonne National Laboratory and the other was passively shielded with 10 cm thick lead bricks. The beam dump was made of tantalum and shielded from the HPGe and Si(Li) detectors with both plastic and lead.

ICEBall consists of six annular Si(Li) detectors that are 5 mm thick and have an active area of 750 mm^2 each. In front of each detector, there is a mini-orange filter which is comprised of a central tungsten absorber surrounded with up to six permanent samarium cobalt magnets. The arrangement of the mini-orange filters has been described in ref. [26]. For each filter 3 permanent magnets were used with field strengths of $\sim$ 900 Gauss at the center and on the surface of the planar magnets. Efficiency and energy calibrations were done using ^{133}Ba and ^{207}Bi sources. Each of these sources were designed to fit on the target ladder within ICEBall. The target was placed at the center of ICEBall through the use of the target ladder. ICEBall has a measured absolute efficiency of 15% at 356 keV and a resolution of 3–5 keV FWHM. An efficiency curve for a single Si(Li) detector is shown in fig. 4.

Energy and efficiency calibrations were performed for the HPGe detectors with the same sources as ICEBall, and were calibrated at the target position. The HPGe detectors from the GEORGINA array had an energy resolution of 1.86 keV FWHM at 356 keV for the ^{133}Ba source. The efficiency calibration is shown in fig. 5. Each HPGe detector had an absolute efficiency of $\sim$ 0.42% at 356 keV for the ^{133}Ba source.

Energy signals were acquired via a Mesytec analog-to-digital converter (MADC-32) module [27]. The timing information was recorded using a Caen V775 [28] time-to-digital converter (TDC) module. In each case, the units were 32 bits. The MESYTEC MADC32 was run with an 8K resolution using 13 bits while the Caen V775 TDC digitizer was run at 4K resolution utilizing 11 bits. The reconstructed timing signals allowed for the separation between the prompt events and the long-lived or random events. For the neutron detectors a Mesytec MPD-4 module [29] was used for pulse shape discrimination.

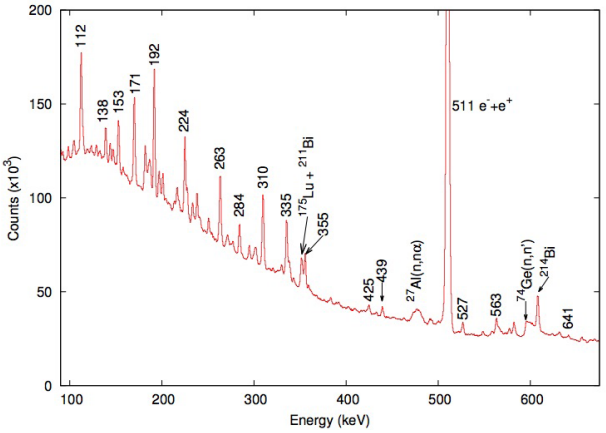

Fig. 6. An ungated gamma spectrum with an active BGO shield. The strongest transitions of ^{176}Lu are labeled and the background peaks that are labeled are from beam induced reactions.

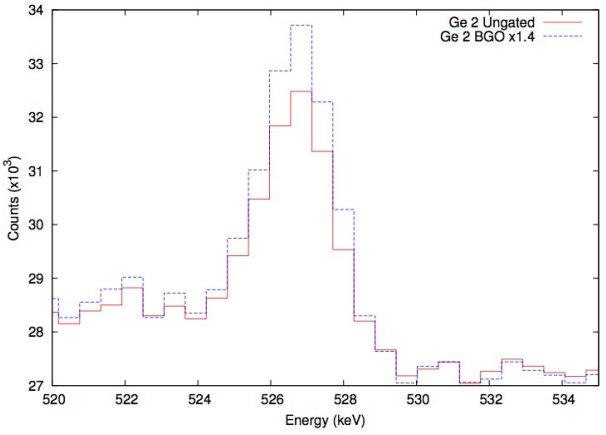

Fig. 7. A comparison between the ungated gamma spectrum *versus* the actively BGO shielded spectrum for the 526 keV γ-ray transition. The peak to background ratio was improved by $\sim$ 20% using the BGO. The scaling factor of 1.4 is normalized from total number of events in the histogram for comparison only.

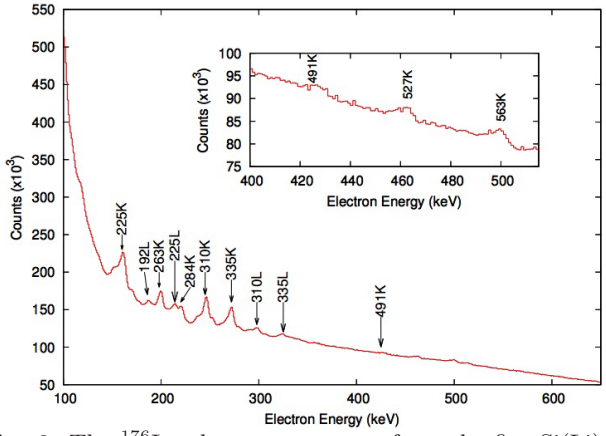

Fig. 8. The ^{176}Lu electron spectrum from the five Si(Li) detector sums.

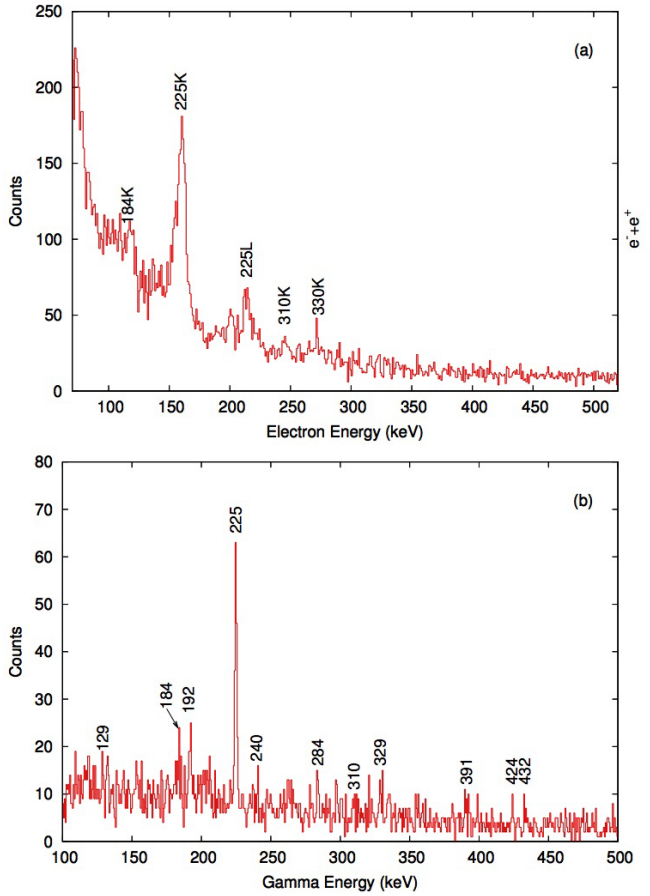

Fig. 9. The γ-ray and electron gates of 310 keV transition. Panel (a) shows the electron spectrum in coincidence with the 310 keV γ-ray transition (all electron peaks are labeled with the energy of the γ-ray transition) whereas panel (b) shows the γ-ray spectrum in coincidence with the electron spectrum.

3 Analysis and results

Figure 6 shows a portion of the singles γ-ray spectra. Our largest source of background was from neutron induced peaks on aluminum. However, once coincidence gates were applied, the neutron induced peaks diminished significantly. The BGO shield on the one HPGe detector led to an improvement of our peak to background ratio by $\sim 20\%$ as shown in fig. 7.

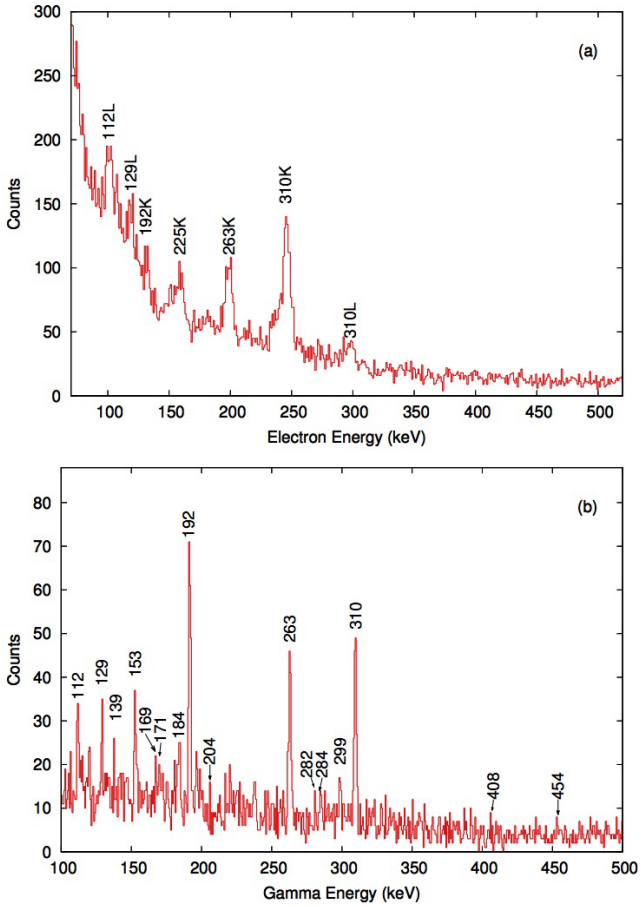

Fig. 10. The γ-ray and electron gates of 225 keV transition. Panel (a) shows the electron spectrum in coincidence with the 225 keV γ-ray transition (all electron peaks are labeled with the energy of the γ-ray transition) whereas panel (b) shows the γ-ray spectrum in coincidence with the electron spectrum.

Five of the six Si(Li) detectors within ICEBall were used and summed together to improve statistics. The summed Si(Li) singles measurement is shown in fig. 8. Due to the density of gamma-rays and limits on detector resolution, only the strongest conversion electrons were detected from the most intense γ-ray transitions.

Gates were set in a ROOT [30] based analysis code on the strongest γ-ray transitions and coincidence relationships were determined from the gated spectra by gamma-gamma and gamma-electron coincidences. Gates were applied to both the gamma and electron spectra.

An example is shown in fig. 9(a), (b) where a gate is set on one of the strongest γ-ray transitions at 310 keV. In the electron spectrum shown in fig. 9(a), we can clearly see a very large K peak for the 225 keV γ-ray transition which is from a direct cascade. The corresponding γ-ray transition is also shown in the gamma coincidence spectrum shown in fig. 9(b).

In fig. 10(a), a 225 keV γ-ray transition gate shows the K conversion peak of the 129 keV γ-ray transition which

Table 1. ^{176}Lu conversion electron energies and gamma rays from this work compared to the ones measured by the BILL spectrometer following the ^{175}Lu(n,γ) reaction [15]. The internal conversion coefficients are given by α and the spin and parity assignments are from [15].

E_{level} (keV)	E_γ	E_e	α		Multipolarity		$J_f^\pi \to J_i^\pi$
			This Work	[15]	This Work	[15]	
184.1	183.0 (3)	119.7	< 0.43 K	0.5	$M1+E2$	$M1+E2$	$8- \to 7-$
235.7	112.14 (13)	101	0.43 (36) L	–	$E2$	$E2$	$3- \to 1-$
299.3	66.23	–	–	12.5	–	$M1+E2$	$3+ \to 2+$
	103.7 (7)	95.1	< 1.69 L	–	$E2$	$E2$	$3+ \to 1+$
305.3	69.49	–	–	10.8	–	$(M1)$	$2- \to 3-$
	181.57 (21)	118.3	< 0.36 K	0.687	$M1$	$M1$	$2- \to 1-$
338.8	105.74	–	–	3.22	–	$M1$	$1+ \to 2+$
	144.0 (3)	133.2	0.31 (26) L	–	$M1+E2$	$M1+E2$	$1+ \to 1+$
372.5	139.1 (16)	128.5	< 1.46 K	0.982	$E2$	$E2$	$4+ \to 2+$
381.3	186.0 (4)	123.0	0.29 (25) K	0.642	$M1$	$M1$	$2+ \to 1+$
386.5	81.30	–	–	6.86	–	$M1$	$1- \to 2-$
	153.46	–	–	0.114	–	$E1$	$1- \to 2-$
	191.5 (1)	128.2	0.12 (6) K	0.0638	$E1$	$E1$	$1- \to 1+$
		182.3	< 0.04 L	–	$E1$	–	$1- \to 1+$
	263.09 (13)	199	0.12 (6) K	0.189	$M1$	$M1+E2$	$1- \to 1-$
388.8	204.75	–	–	0.44 (3)	–	$M1+E2$	$9- \to 8-$
433.0	46.45	–	–	6.42	–	$M1+E2$	$2- \to 1-$
	197.26	–	–	0.164	–	$M1$	$2- \to 3-$
	309.66 (10)	246.4	0.11 (5) K	0.160	$M1$	$M1$	$2- \to 1-$
		299.5	0.024 (10) L	–	$M1$	–	$2- \to 1-$
437.3	201.4 (3)	138.1	0.6 (5) K	0.275	$E2$	$E2$	$5- \to 3-$
463.7	227.13 (18)	163.8	0.40 (28) K	0.355	$M1+E2$	$M1+E2$	$4- \to 3-$
487.6	187.6 (3)	124.3	0.33 (30) K	0.345	$E2$	$E2$	$5+ \to 3+$
591.7	219.28	–	–	0.208	–	$E2$	$6+ \to 4+$
613.4	224.66 (16)	161.6	0.8 (7) K	–	$(M1)$	$M1$	$10- \to 9-$
635.2	147.55	–	–	1.24	–	$M1$	$4+ \to 5+$
	253.85	–	–	0.129	–	$E2$	$4+ \to 2+$
	335.2 (3)	271.9	0.14 (7) K	–	$M1$	$M1+E2$	$4+ \to 3+$
		324.3	< 0.11 L	–	$M1$	–	$4+ \to 3+$
637.7	204.74	–	–	0.499	–	$M1$	$1- \to 2-$
	250.6 (6)	186.8	0.38 (25) K	0.284	$M1$	$M1$	$1- \to 1-$
657.1	284.43	221.1	0.18 (8) K	0.202	$M1$	$M1$	$5+ \to 4+$
	170.2 (5)	106.9	< 1.09 K	–	$M1, E2$	$(M1, E2)$	$5+ \to 5+$
		159.2	< 0.81 L	–	$M1, E2$		$5+ \to 5+$
658.4	224.67 (20)	161.4	0.38 (24) K	0.369	$M1+E2$	$M1+E2$	$3- \to 2-$
	271.86	–	–	0.104	–	$(E2)$	$3- \to 1-$
	422.67	–	–	0.0701	–	$M1$	$3- \to 3-$
709.2	221.3	–	–	0.402	$M1$	$M1$	$(7+) \to 8+$
710.1	272.4 (4)	209.2	0.33 (21) K	0.227	$M1$	$M1$	$6- \to 5-$
734.0	309.10 (15)	245.8	0.21 (13) K	0.161	$M1$	$(M1)$	$(7+) \to 8+$
788.2	129.4 (9)	119.1	< 1.07 L	–	$M1$	$M1$	$4- \to 3-$
796.6	491.5 (6)	428.2	0.022 (1) K	0.0476	$M1$	$M1$	$1- \to 2-$
838.6	115.7	–	–	2.49	–	$(M1)$	$5- \to 4-$
	274.70	–	–	0.223	–	$M1$	$5- \to (6)-$

Table 1. Continued.

E_{level} (keV)	E_γ	E_e	α		Multipolarity		$J_f^\pi \rightarrow J_i^\pi$
			This Work	[15]	This Work	[15]	
	838.62	–	–	0.00567	–	$E2$	$5- \rightarrow 7-$
866.4	433.32	–	–	0.00865	–	$E1$	$2+ \rightarrow 2-$
	485.00	–	–	0.0492	–	$M1$	$2+ \rightarrow 2+$
	527.23 (22)	463.9	0.06 (3) K	0.0399	$M1$	$M1$	$2+ \rightarrow 1+$
883.5	419.70	–	–	0.0714	–	$M1$	–
	578.3 (3)	513.9	0.015 (14) K	0.0315	$M1$	$M1$	$3- \rightarrow 2-$
973.7	336.6 (15)	275.3	0.15 (9) K	0.126	$M1$	$M1$	$5+ \rightarrow 4+$
985.5	250.6 (4)	187.3	0.18 (12) K	0.284	$M1$	$M1$	$4+ \rightarrow 3+$
	349.9 (6)	286.6	< 0.29 K	0.115	$(M1)$	$M1$	$4+ \rightarrow 4+$
	328.04 (19)	270	0.2 (1) K	0.137	$M1$	$M1$	$4+ \rightarrow 5+$
		318	0.07 (6) L	–	$M1$	–	$4+ \rightarrow 5+$
1015.3	564.2 (3)	500.9	< 0.05 K	0.0334	$M1$	$M1$	$4+ \rightarrow 3+$
	642.89	–	–	0.0102	–	$(E2)$	$4+ \rightarrow 4+$
1019.9	284.3 (3)	221.0	0.58 (44) K	–	$M1, M2$	–	$(1-, 2+, 4+, 5-) \rightarrow 3+$
1029.6	524.82	–	–	0.0404	–	$M1$	$(2-) \rightarrow 3-$
	596.63	–	–	0.0291	–	$M1$	$(2-) \rightarrow 2-$
	643	581		–	–	–	–
		633	< 14 K/L	–	$M1 + E2$	$M1(+E2)$	$(2-) \rightarrow 1-$
1032.4	197.54	–	–	0.551	–	$(M1)$	$6- \rightarrow (5-)$
	309.5 (2)	246.1	0.038 (29)	–	$E2$	–	$6- \rightarrow 4-$
1118.8	262.1 (3)	198.8	0.10 (7) K	–	$M1$	–	$12- \rightarrow 11-$
1164.1	321.2 (8)	258.6	< 0.34 K	–	$M2$	–	$(1+, 5+) \rightarrow 3-$
1277.8	439.3 (4)	376.0	0.04 (2) K	–	$M1$	–	$(4-, 6-) \rightarrow 5-$
1301.4	566.1 (5)	502.8	0.013 (12) K	–	$M1$	–	$(2+, 4+) \rightarrow 3+$

is indistinguishable in the raw electron spectrum, but is clearly seen in the gated electron spectrum. The same 225 keV γ-ray transition was gated on the corresponding gamma spectrum for gamma-gamma coincidences and is shown in fig. 10(b). All of these transitions were verified in the corresponding level schemes shown in fig. 11(a).

Another gamma ray transition was placed on the 263 keV γ-ray transition and in the electron spectrum we are able to measure both the 643K and 643L conversion electrons as shown in fig. 12(a). In the corresponding gated gamma-gamma spectrum shown in fig. 12(b), the 643 keV line is too weak to yield a conversion coefficient using the ratio of electrons over gammas. However, since both the K and L electrons are much stronger, we are able to still measure a conversion coefficient using the ratio of K/L. Each of the γ-ray transitions were verified in the corresponding level schemes shown in fig. 11(b).

A gate on the 335 keV γ-ray transition and the electron spectrum is shown in fig. 13(a). The gamma-gamma coincidences are shown in fig. 13(b). Each of the γ-ray transitions were verified in the corresponding level schemes shown in fig. 11(c).

A total of 42 conversion coefficients were measured where 17 of them have been measured for the first time in this work. The results are shown in table 1 along with previous measurements. If the gamma-ray energy was determined for the first time by this work, we indicated the error in the energy. Both electron and gamma-ray energies carried errors due to statistics.

The conversion coefficients from this work were compared to previous results from Klay *et al.* [15]. The level structure used was established through the work of Klay *et al.* (^{175}Lu(n,γ)) [15] and additional (n,γ) experiments [31,32], Dracoulis *et al.* (^{176}Lu + ^{136}Xe inelas-

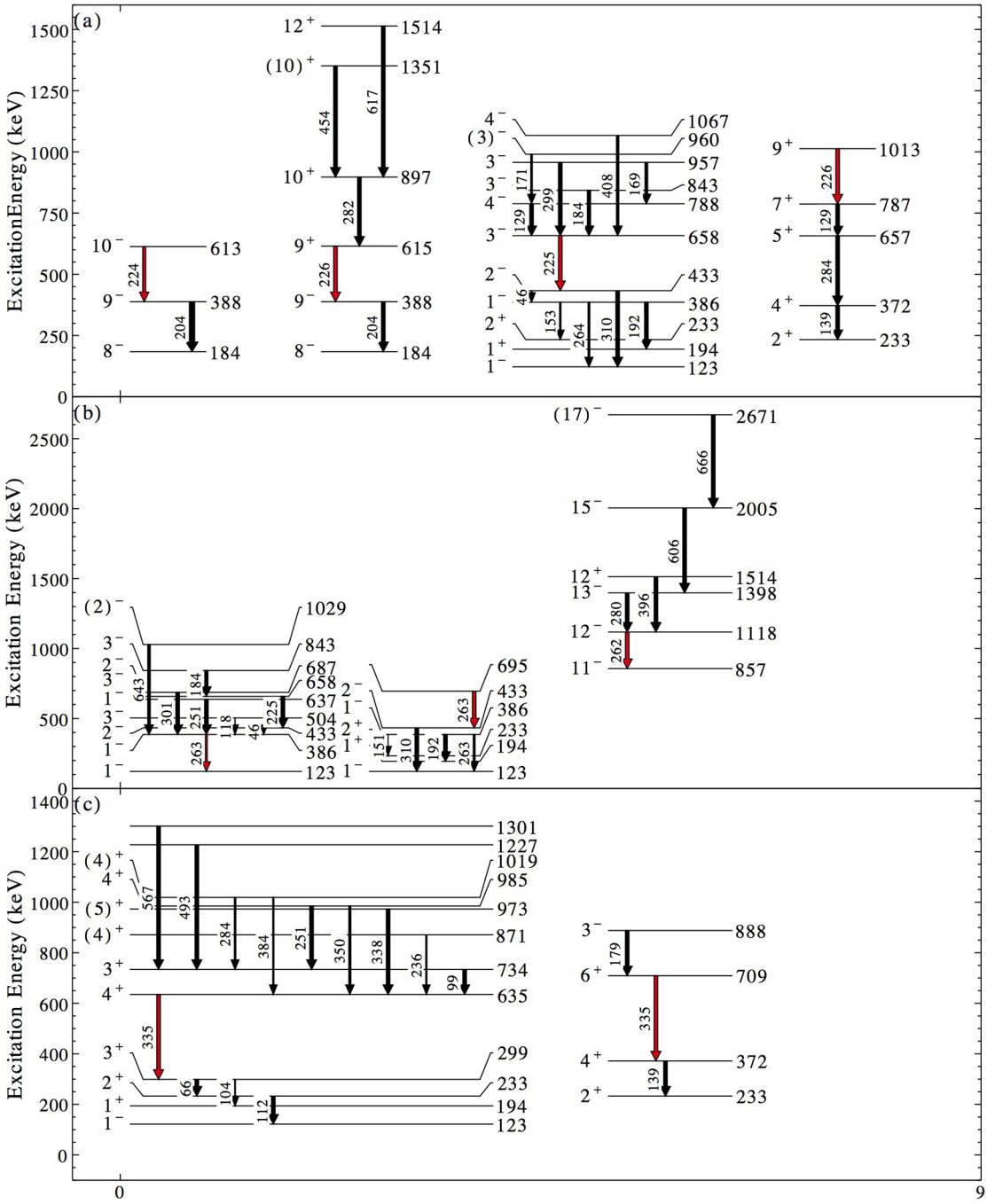

Fig. 11. (a) Level scheme for the gamma gate at 225 keV showing the coincidence gammas. (b) Level scheme for the gamma gate at 263 keV showing the coincidence gammas. (c) Level scheme for the gamma gate at 335 keV showing the coincidence gammas. Created with SciDraw [33].

tic reaction) [9], McGoram *et al.* (^{176}Yb(^{7}Li, $\alpha 3n$)) [16], Lesko *et al.* (^{176}Yb(p,n)) [13], and Dewberry *et al.* (^{177}Hf(t,α)) [34]. BRICC [35] was used to compare the measured conversion coefficients to the theoretical conversion coefficients. Using BRICC and the current level assignments, multipolarities were assigned for all measured conversion coefficients. For the conversion electrons that were difficult to measure (*e.g.* low statistics) an upper bound was determined. If there was no spin assignment previously, only the multipolarity of the transition was determined. The large electron background and low electron efficiency at < 100 keV (shown in fig. 4) conversion coefficients could be established with sufficiently high statistics. A large number, 28 conversion coefficients, were consistent with the previous measurements and spin assignments. The 973.7 keV level spin verified the proposed

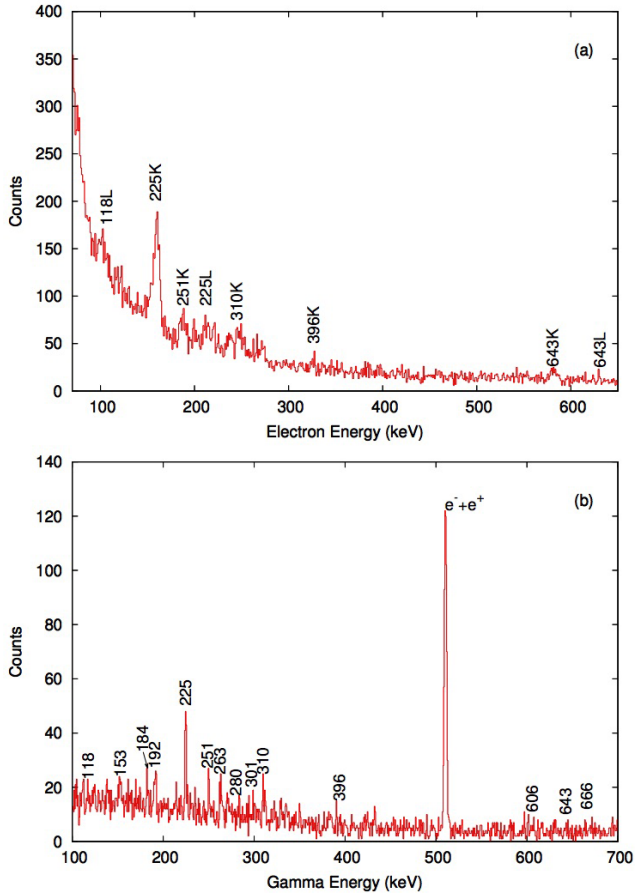

Fig. 12. The γ-ray and electron gates of 263 keV transition. Panel (a) shows the electron spectrum in coincidence with the 263 keV γ-ray transition (all electron peaks are labeled with the energy of the γ-ray transition) whereas panel (b) shows the γ-ray spectrum in coincidence with the electron spectrum.

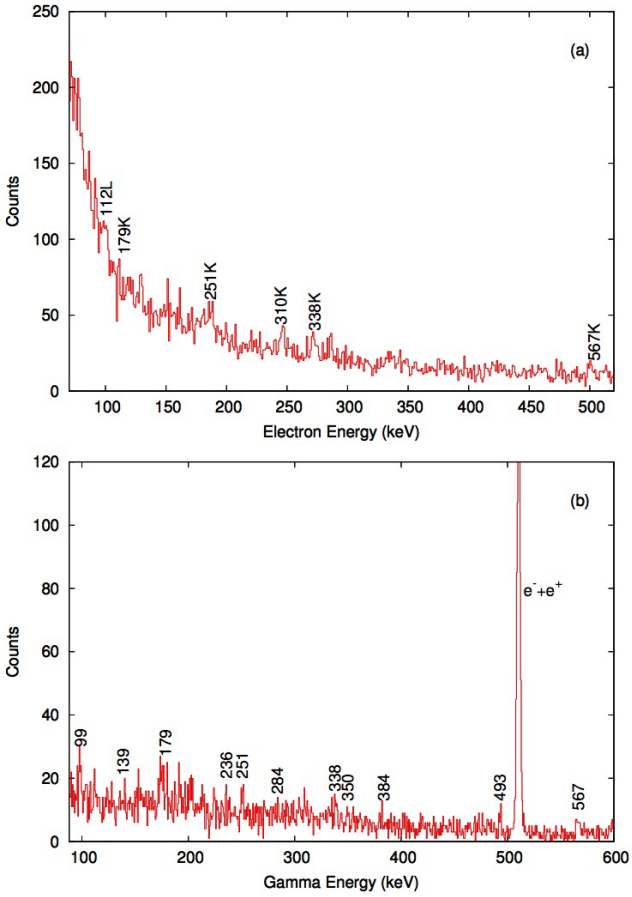

Fig. 13. The γ-ray and electron gates of 335 keV transition. Panel (a) shows the electron spectrum in coincidence with the 335 keV γ-ray transition (all electron peaks are labeled with the energy of the γ-ray transition) whereas panel (b) shows the γ-ray spectrum in coincidence with the electron spectrum.

5^+ spin assignment. However, with three conversion coefficient measurements, there is a disagreement with the previous spin assignments by Klay *et al.* [15]. Here we measure conversion coefficients and can assign a multipolarity for the transition. For example, the 1019.9 keV level seen by [15], our conversion coefficient shows evidence that the transition should either be $M1$ or $M2$. The conversion coefficient for the 1032.4 keV level indicates a 6^- instead of the proposed (5^-). Three levels have no previous spin assignments, however conversion coefficients were measured for these levels. The 1164.1 level spin from the conversion coefficient indicates a spin of 1^+ or 5^+. In addition the spin of the 1277.8 level indicates either a 4^- or 6^- spin assignment from the conversion coefficient. The 1301.4 level spin from the conversion coefficient indicates either a 2^+ or 4^+ spin assignment.

In this work, 35 new multipolarity assignments were made, however, no new intermediate states were found beyond those already established by Dracoulis *et al.* [9]. Due to the low intensity of the intermediate state such as the 839 keV level with a $< 10\%$ branching [13] we did not see them. Despite the fact that no new intermediate states were identified, transitions that depopulate the intermediate states were verified and conversion coefficients were measured in order to extract their multipolarities. One such state is the level at 635 keV which is connected to the 709 keV state [9]. The initial determination of the multipolarity of that transition was $M1 + E2$ [15], however the new multipolarity is constrained to $M1$ through the measurement of our conversion coefficients. In the $K^\pi = 4^+$ band, 3 transitions from the $K^\pi = 4^+$ were identified and the corresponding conversion coefficients verified the spin assignments and the partial level scheme is shown in fig. 14 with the boxed transitions indicating our measured conversion coefficients. In the $K^\pi = 4^-$ band from the identification of Klay *et al.*, 2 transitions were identified and from the corresponding conversion coefficients the spin assignments were verified. The partial level scheme of $K = 4^-$ band is shown in fig. 15 with the boxed transitions indicating our measured conversion coefficients. The spin assignments that were verified in both the $K = 4^+$ and $K = 4^-$ band help complete the nuclear structure relevant to the intermediate states that are important for the production of ^{176}Lu in stellar environments.

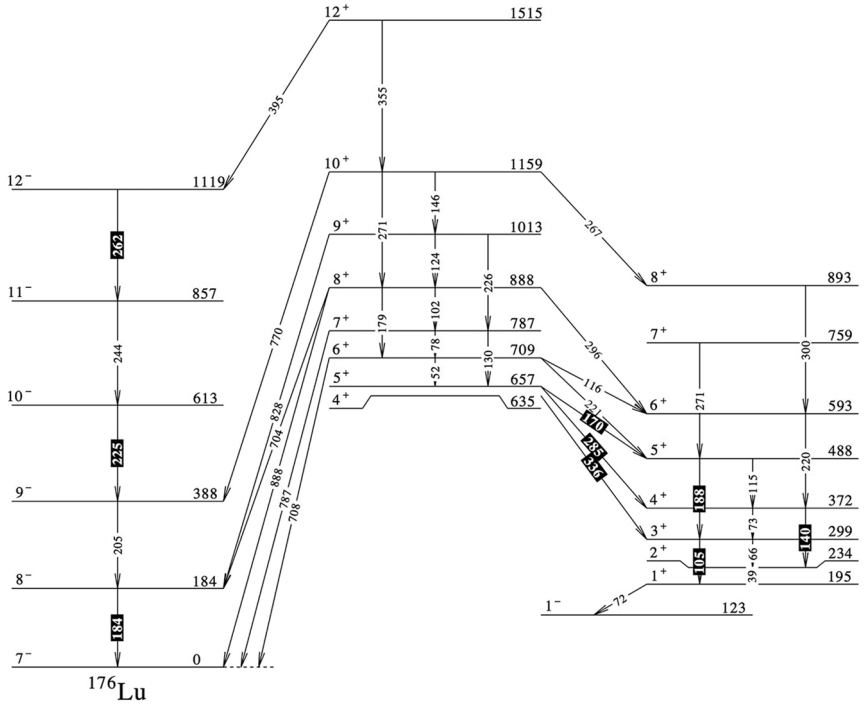

Fig. 14. Partial level scheme for $K^\pi = 4^+$ band from Dracoulis *et al.* [9] that we see in the present work. The boxed transition energies highlight the measured spin assignments in this work. Created with SciDraw [33].

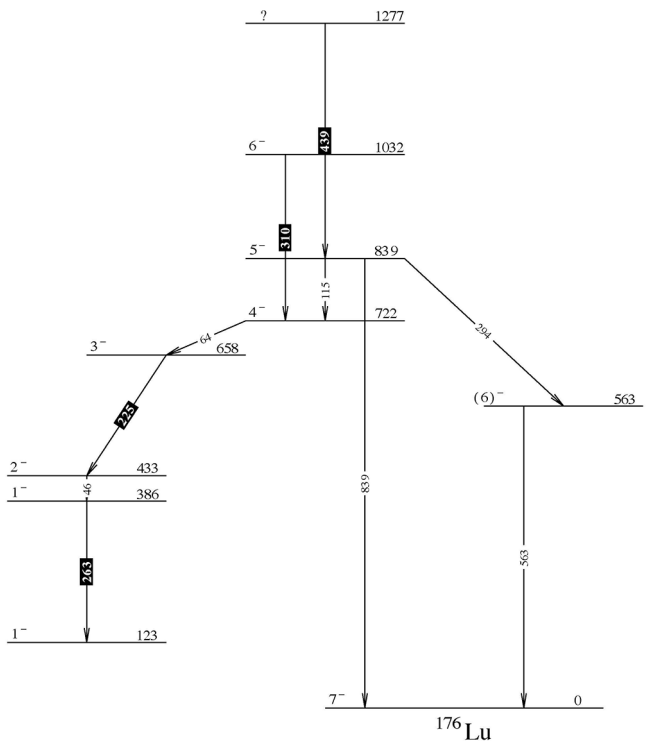

Fig. 15. Partial level scheme for $K^\pi = 4^-$ band from Klay *et al.* [15] that we see in the present work. The boxed transition energies highlight the measured spin assignments in this work. Created with SciDraw [33].

4 Conclusions

Conversion coefficients were measured for states in ^{176}Lu via a ^{176}Yb(p, n) reaction at 7.75 MeV at the NSL of the University of Notre Dame. A total of 42 conversion coefficients were measured through gamma-gamma and gamma-electron coincidences using ICEBall and two HPGe detectors (109% relative efficiency) from the GEORGINA array. A total of 17 conversion coefficients were measured for the first time in this work, we have additionally made 35 multipolarity assignments. No new intermediate states were observed however, the transition multipolarities of the intermediate states populating and depopulating both $K = 4^+$ and $K = 4^-$ states were measured. The intermediate states are the ones that can affect the final abundance of ^{176}Lu. The implications are broad with potential impact as far reaching as the r-process abundance distributions.

This work was supported by the National Science Foundation under contract numbers PHY-1068192 and PHY-1419765. We also appreciate Gulhan Gurdal for her assistance for dismantling ICEBall at the Wright Nuclear Structure Laboratory at Yale University. We gratefully acknowledge discussions with George Dracoulis that led to this work.

References

1. F. Käppeler, Prog. Part. Nucl. Phys. **43**, 419 (1999).
2. F. Käppeler, R. Gallino, S. Bisterzo, W. Aoki, Rev. Mod. Phys. **83**, 157 (2011).

3. M. Heil, N. Winckler, S. Dababneh, F. Käppeler, K. Wisshak, S. Bisterzo, R. Gallino, A.M. Davis, T. Rauscher, Astrophys. J. **673**, 434 (2008).
4. M. Arnould, S. Goriely, K. Takahashi, Phys. Rep. **450**, 97 (2007).
5. National Research Council, *Connecting Quarks with the Cosmos: Eleven Science Questions for the New Century* (National Academies Press, 2003).
6. C. Sneden, J.J. Cowan, J.E. Lawler, I. Ivans, S. Burles, T.C. Beers, F. Primas, V. Hill, J.W. Truran, G.M. Fuller, Astrophys. J. **591**, 936 (2003).
7. M. Mumpower, R. Surman, G.C. McLaughlin, A. Aprahamian, Prog. Particle Nucl. Phys. **87**, 116 (2016).
8. V. Gintautas, A.E. Champagne, F.G. Kondev, R. Longland, Phys. Rev. C **80**, 015806 (2009).
9. G.D. Dracoulis, F.G. Kondev, G.J. Lane, A.P. Byrne, M.P. Carpenter, R.V.F Janssens, T. Lauritsen, C.J. Lister, D. Seweryniak, P. Chowdhury, Phys. Rev. C **81**, 011301(R) (2010).
10. F.G. Kondev, G.D. Dracoulis, T. Kibédi, At. Data Nucl. Data Tables **103-104**, 50 (2015).
11. J. Audouze, W.A. Fowler, D.N. Schramm, Nature **238**, 8 (1972).
12. J. Laeter, N. Bukilic, Phys. Rev. C **73**, 045806 (2006).
13. K.T. Lesko, E.B. Norman, R.M. Larimer, B. Sur, Phys. Rev. C **44**, 2850 (1991).
14. H. Beer, F. Käppeler, K. Wisshak, Astrophys. J. Suppl. Ser. **46**, 295 (1981).
15. N. Klay, F. Käppeler, H. Beer, G. Schatz, H. Börner, F. Hoyler, S.J. Robinson, K. Schreckenbach, B. Krusche, U. Mayerhofer, G. Hlawatsch, H. Lindner, T. vonEgidy, W. Andrejtscheff, P. Petkov, Phys. Rev. C **44**, 2801 (1991).
16. T.R. McGoram, G.D. Dracoulis, T. Kibédi, A.P. Byrne, R.A. Bark, A.M. Baxter, S.M. Mullins, Phys. Rev. C **62**, 031303(R) (2000).
17. W.R. Zhao, F. Käppeler, Phys. Rev. C **44**, 506 (1991).
18. H. Beer, F. Käppeler, Phys. Rev. C **21**, 534 (1980).
19. J.R. DeLaeter, B.J. Allen, G.C. Lowenthal, J.W. Boldeman, J. Astrophys. Astron. **9**, 7 (1988).
20. C. Doll, H.G. Börner, S. Jaag, F. Käppeler, W. Andrejtscheff, Phys. Rev. C **59**, 492 (1999).
21. M. Scheck *et al.*, Phys. Rev. C **75**, 044313 (2007).
22. P. Mohr, S. Bisterzo, R. Gallino, F. Käppeler, U. Kneissl, N. Winckler, Phys. Rev. C **79**, 045804 (2009).
23. J. Vanhorenbeeck, J. Lagrange, M. Pautrat, J. Dionisio, Ch. Vieu, Phys. Rev. C **62**, 015801 (2000).
24. M.P. Metlay, *Development of a Multiple-Element Conversion-Electron Spectrometer Array and Investigation of Transition Multipolarities in* ^{130}*Ce*, PhD Thesis, University of Pittsburgh (1992).
25. A.M. Baxter *et al.*, Nucl. Instrum. Methods Phys. Res. A **317**, 101 (1992).
26. M.P. Metlay, J.X. Saladin, I.Y. Lee, O. Dietzch, Nucl. Instrum. Methods Phys. Res. A **336**, 162 (1993).
27. MESYTEC, *MADC-32 V2.1*, `http://www.mesytec.com/datasheets/MADC-32.pdf`.
28. CAEN, *Caen V775*, `http://www.caen.it/`.
29. MESYTEC, *MPD4*, `http://www.mesytec.com/datasheets/MPD-4.pdf`.
30. R. Brun, F. Rademakers, Nucl. Instrum. Methods Phys. Res. A **389**, 81 (1997).
31. R.W. Hoff, R.F. Casten, M. Bergoffen, D.D. Warner, Nucl. Phys. A **437**, 285 (1985).
32. O. Wasson, R. Chrien, Phys. Rev. C **2**, 675 (1970).
33. M.A. Caprio, Comput. Phys. Commun. **171**, 107 (2005).
34. R.A. Dewberry, R.K. Sheline, R.G. Lanier, L.G. Mann, G.L. Struble, Phys. Rev. C **24**, 1628 (1981).
35. T. Kibédi, T.W. Burrows, M.B. Trzhaskovskaya, P.M. Davidson, C.W. Nestor jr., Nucl. Instrum. Methods Phys. Res. A **589**, 202 (2008).